Three-point statistics and the anisotropy of a turbulent passive scalar

Cite as: Physics of Fluids **10**, 2885 (1998); https://doi.org/10.1063/1.869809
Submitted: 06 May 1998 . Accepted: 20 July 1998 . Published Online: 06 October 1998

L. Mydlarski, and Z. Warhaft

Three-point statistics and the anisotropy of a turbulent passive scalar

L. Mydlarski[a] and Z. Warhaft
Sibley School of Mechanical and Aerospace Engineering, Cornell University, Ithaca, New York 14853

(Received 6 May 1998; accepted 20 July 1998)

The mixing of passive scalar (temperature) fluctuations produced by the action of a mean temperature gradient in decaying isotropic grid-generated turbulence is studied experimentally for the range $200<R_\lambda<500$. Previously, the observed anisotropy of the small scale (inertial range) scalar fluctuation statistics has been described in terms of two-point structure functions. Here we map the three-point cross-correlation and structure functions. We show that they exhibit universal characteristics. These are related to the ramp-cliff morphology that is ubiquitous to all flows with mean gradients of a passive scalar. © *1998 American Institute of Physics.* [S1070-6631(98)01211-2]

I. INTRODUCTION

In 1941, Kolmogorov[1,2] predicted (in the limit of infinite Reynolds number) the scaling of the structure functions of velocity for the inertial subrange, i.e., the range of scales between the largest (energy containing) and smallest (dissipation) scales. The predictions rely on the hypothesis of local isotropy, i.e., that the statistics of the turbulence are invariant to rotations and reflections of the coordinate system. At the level of second order statistics, the local isotropy assumption has been very successful. Thus it has been found[3,4] that if the Reynolds number is high enough to provide a substantial inertial subrange, then the ratio of transverse to longitudinal velocity variances are consistent with local isotropy both in the inertial and dissipation ranges. For higher order statistics, the Kolmogorov 1941 (K41) theory had to be modified in order to take internal intermittency into account. This is the subject of the refined similarity hypothesis (RSH) (Refs. 5, 6) that has received much attention, and as yet does not have a theoretical closure. (For summaries, see Frisch[7] and Nelkin.[8]) Like K41, the RSH assumes local statistical isotropy, yet there is strong evidence[9–11] that for statistical moments of higher order than two, small-scale anisotropy persists at least to moderately high Reynolds numbers. Whether this tendency extends to the highest Reynolds numbers is still unclear.

Extension of the Kolmogorov 1941 theory to the mixing of a passive scalar by a turbulent flow was done by Oboukhov[12] and Corrsin[13] and the RSH has also been extended to the scalar.[14,15] Scaling arguments, similar to those for the velocity field, were derived assuming local isotropy of the scalar field. Yet this assumption has been found to be contradicted (experimentally and numerically) by many researchers.[16–22] The violation is primarily observed by nonzero odd-order statistics in both the inertial and dissipative ranges. In particular, the skewness of the scalar derivative (along the mean gradient) has been found to be of order one.[16,18–22] The measurements, both in shear flows,[16,18] and isotropic turbulence[20] extend to high Reynolds number ($R_\lambda \sim 10^3$). Local isotropy (in the high-Reynolds-number limit) predicts that the skewness should be zero. These, and observations of the anomalous behavior of the odd-order structure functions[17,20] to be discussed below, constitute a serious flaw to the most widely accepted theory of the turbulent mixing of a passive scalar and are therefore of particular interest.

The flaw in basic Kolmogorov phenomenology is best described in terms of the third-order structure function of the scalar

$$\langle \Delta\theta(r)^3\rangle \equiv \langle (\theta(r)-\theta(0))^3\rangle, \tag{1}$$

where θ is the fluctuating (passive) temperature (about a local mean T) and the difference is taken in the direction of the mean temperature gradient (β). [In the experiment to be described here, the flow is in the x-direction, y is transverse to x and $\beta \equiv dT/dy$. Moreover, β is constant (or approximately so; see Sec. II) and the velocity field is approximately isotropic. This is the simplest realization of a scalar field in turbulent flow.] For large r (i.e., on the order of an integral scale), the existence of (1) is expected. Its value (caused by β) would be a perturbation about the isotropic background state. As the separation decreases, $\langle \Delta\theta(r)^3\rangle$ should approach zero if there is sufficient separation between the integral and dissipation scales (i.e., if the Reynolds number is large enough). If we assume to first order that $\langle \Delta\theta(r)^3\rangle$ is proportional to β, then the Kolmogorov mixing argument suggests that

$$\langle \Delta\theta(r)^3\rangle = \beta f(\epsilon, \epsilon_\theta, r), \tag{2}$$

where the separation r is taken in the direction of a mean temperature gradient, and ϵ and ϵ_θ are the dissipation rate of turbulent kinetic energy and smearing rate of temperature fluctuations, respectively. Dimensional considerations then necessitate that

$$\langle \Delta\theta(r)^3\rangle \propto \beta \epsilon^{-1/3} \epsilon_\theta r^{5/3}. \tag{3}$$

Note that since $\epsilon_\theta \propto \beta^2$, this expression scales as β^3, as it must, since the convective-diffusive equation is linear in θ.

[a]Present address: Department of Mechanical Engineering, McGill University, Montréal, Québec, Canada.

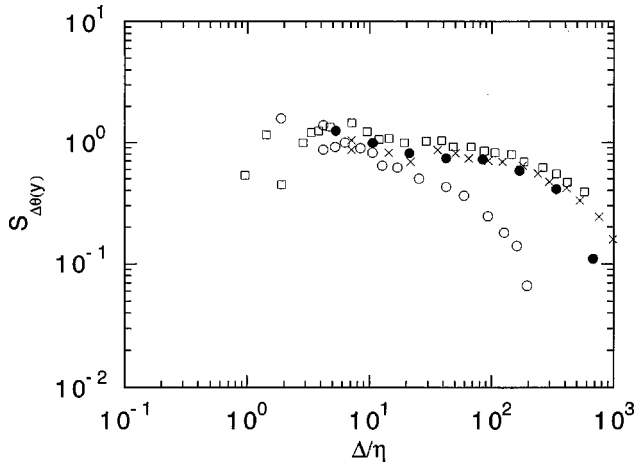

FIG. 1. Normalized transverse temperature skewness structure functions $\langle(\Delta_y\theta)^3\rangle/\langle(\Delta_y\theta)^2\rangle^{3/2}$ plotted as a function of the separation scaled by the Kolmogorov length scale, $\eta=(\nu^3/\epsilon)^{1/4}$. Apart from the solid circles, the data is from Mydlarski and Warhaft (1998) (Ref. 20). Open circles are for $R_\lambda=99$. Squares are for $R_\lambda=222$. Crosses are for $R_\lambda=461$. Solid circles are for the experiments to be described below; $R_\lambda=247$ (horizontal tunnel, synchronous mode). Note that the scaling range (horizontal region) does not occur for the low R_λ case.

The argument leading to (3) is similar to that used to predict the form of the Reynolds stress spectrum by Lumley.[23] There it is assumed that the anisotropic perturbation caused by the Reynolds stress is proportional to the velocity gradient.

The third-order structure function can be normalized by the second-order structure function $\langle\Delta\theta(r)^2\rangle$. Using (3) and Kolmogorov form for the second order structure function, $\langle(\theta(r)-\theta(0))^2\rangle\propto\epsilon^{-1/3}\epsilon_\theta r^{2/3}$, the prediction for the skewness structure function is

$$S_{\Delta\theta(r)}\equiv\frac{\langle\Delta\theta(r)^3\rangle}{\langle\Delta\theta(r)^2\rangle^{3/2}}\propto\beta\epsilon^{-1/6}\epsilon_\theta^{1/2}r^{2/3}. \tag{4}$$

Figure 1, which includes data from Mydlarski and Warhaft, 1998 (Ref. 20) (from here on referred to as M&W) shows $S_{\Delta\theta(y)}$ for wind tunnel turbulence experiments in close to isotropic grid turbulence with a mean temperature profile. It is quite evident that the scaling exponent (for high Reynolds numbers) is close to zero; not 2/3 as predicted by (4). A similar departure from Kolmogorov scaling was earlier reported by Antonia and Van Atta[17] for the third-order structure function in shear flows. As mentioned above, M&W also showed that the skewness of the temperature derivative along the mean temperature gradient,

$$S_{\partial\theta/\partial y}\equiv\frac{\langle(\partial\theta/\partial y)^3\rangle}{\langle(\partial\theta/\partial y)^2\rangle^{3/2}} \tag{5}$$

is of order one and does not decrease with Reynolds number. Kolmogorov reasoning (in the same vein as presented above for the third-order structure function) predicts that $S_{\partial\theta/\partial y}\propto R_\lambda^{-1}$, where R_λ is the turbulent Reynolds number based on the Taylor-microscale. It is these pronounced departures from expected phenomenology that motivate the present work.

The anomalous scalar behavior is due to ramp-cliff structures of the scalar that align themselves with the mean gradient.[16–22] They persist even as the Reynolds number increases, and the sharp cliffs affect the small scale statistics. Since they manifest themselves in third (and higher order) statistics, their morphology must be examined in terms of three-point structure and correlation functions. There have been no previous experimental attempts along these lines. Recent theoretical and numerical work by Shraiman, Siggia, and Pumir[24–27] on the three-point correlations indicate that the anisotropic scalar structure seems to have universal characteristics that appear to be independent of the nature of the random velocity field. It is the purpose of this paper to experimentally examine this problem.

II. APPARATUS

The experiments were conducted in our two low-speed, low-background-turbulence open circuit wind tunnels. The vertical wind tunnel is 40.65×40.65 cm^2 in cross section and 4.5 m long while the horizontal wind tunnel is 91.44×91.44 cm^2 in cross section and 9.1 m long. They are, respectively, described, with sketches, in Refs. 28 and 29.

The turbulence was generated by means of an active grid following the design of Makita.[30] The active grid is composed of rotating grid bars to which are attached triangular agitator wings. Stepper motors, located at the end of each grid bar outside of the tunnel, rotate the bars. The speed of the grid bar rotation is determined by a square-wave fed to the motor. Detailed descriptions of the grids used in each tunnel can be found in Refs. 4 and 20.

Nearly all of the experiments described here were conducted in our vertical wind tunnel. The data set which was most analyzed was for $R_\lambda=213$ with the active grid operating in synchronous mode—all grid bars rotated at a constant speed and a bar's (constant) direction of rotation was reversed from bar to bar so as not to add net vorticity to the flow. The initial condition for the grid in the vertical tunnel was set so that all wings on bars oriented in the North–South direction were vertical and all of the East–West wings were horizontal. The relative orientation of the grid bars in synchronous mode did not change over the measurement period. Measurement of the three-point correlation at the higher R_λ of 469 was done with the grid in what we call random mode, where the direction of rotation of an individual grid bar randomly changes. [Some three-point structure functions (Fig. 10, below) were also measured in our horizontal wind tunnel at $R_\lambda=564$.] Though the random mode generated a higher turbulent Reynolds number for a given mean velocity {by increasing both the turbulence intensity, $\langle u^2\rangle^{1/2}/U$ [where u is the fluctuation in the longitudinal (x-direction) velocity about the mean longitudinal velocity, U] and the integral length scale, l}, it resulted in a significant decay in the mean temperature gradient, due to the large scalar integral scale, which approached that of the tunnel width.[20] It will be shown, however, that the mode of operation of the grid produced similar results, be it in synchronous or random mode.

The mean cross-stream temperature gradient was produced by a *toaster*, a set of parallel, differentially heated ribbons at the entrance to the settling chamber of the tunnel. Once the flow has passed through the screened plenum and

contraction, the wakes (of both momentum and temperature) created by the toaster elements are smoothed out. This results in a mean temperature profile in the (almost) laminar region upstream of the grid. The flow then passes through the active grid and thermal fluctuations are produced by the turbulence acting against the temperature profile.

The velocity and temperature fluctuations were measured using TSI 1210 probes. For the velocity measurements, tungsten wires of 3.05 μm diam with a length to diameter ratio of approximately 200 were operated at an overheat of 1.8 using Dantec 55M01 constant-temperature anemometers. Tunnel and electronic noise were subtracted from the spectra on a mean-square basis. Spatial resolution corrections for wire length were made using the method of Wyngaard.[31] For temperature measurements, platinum resistance wires of 0.63 μm diam were used. Their length to diameter ratio, L/d_w, where L, is the etched length of the wire and d_w is the wire diameter, varied between 500–600. The minimum prong spacing was roughly $3L$. They were operated at low overheat (probe current approximately 250 μA) to minimize contamination by velocity. Our fast-response DC temperature bridges were based on the design of Haughdal and Lienhard.[32] Electronic and ambient thermal noise were subtracted from the spectra on a mean-square basis. Spatial resolution corrections for wire length were made using the method of Wyngaard.[33] Further details can be found in M&W.[20]

For cold-wire lengths of $L/d_w < 1500$, Browne and Antonia[34] show that heat conduction between a cold-wire and its stubs and/or prongs is a significant source of error in the moments of temperature and its time derivative. Unfortunately, minimization of this error by use of a longer wire results in an increase in error from the reduced spatial resolution of the wire. It was concluded in M&W (Ref. 20) that for this flow, the wire lengths used were appropriate, given the competing effects of wire-prong conduction and reduced spatial resolution.

All signals were high and low pass filtered and digitized with a 12 bit A/D converter. 3×10^6–4×10^6 samples were taken (i.e., 750–1000 blocks each composed of 4096 samples) for each data record at intervals roughly on the order of a Kolmogorov time period to ensure both a fine temporal resolution of the signal (and therefore a signal well resolved spatially in the longitudinal direction) and convergence of the three-point statistics. The only exception to this is for some data included in Figs. 10(a) and 10(b) measured in our horizontal wind tunnel where 150–200 blocks of data were recorded. 4×10^5 data points were sufficient for the power spectra in Fig. 2 where the data were sampled at over twice the Kolmogorov frequency.

III. RESULTS

A remarkable aspect of passive scalars in grid-generated turbulence is that their statistics are well developed at low Reynolds numbers.[19,20] Thus even by a Reynolds number, $R_\lambda \equiv u\lambda/\nu \sim 100$ (where u is the r.m.s. of the longitudinal velocity fluctuations, λ is the Taylor microscale, and ν is the kinematic viscosity), the spectrum has a clear scaling region,

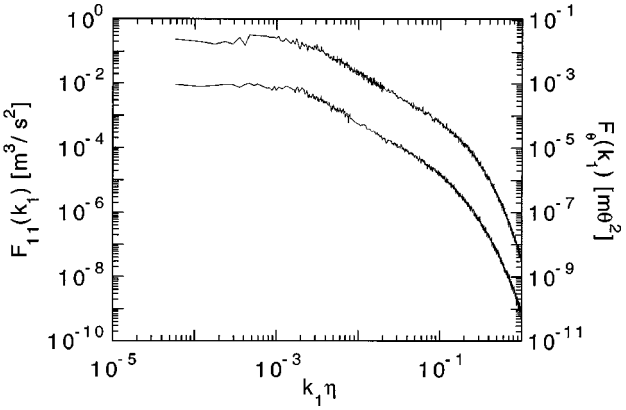

FIG. 2. Power spectra of the longitudinal velocity fluctuations (u, lower curve) and temperature fluctuations (θ, upper curve) for $R_\lambda = 247$ (horizontal tunnel, synchronous mode). k_1 is the longitudinal wave number $= 2\pi f/U$. η is the Kolmogorov length scale $= (\nu^3/\epsilon)^{1/4}$.

the intermittency exponent is high[20] ($\mu_\theta \sim 0.2$–0.25) and the conditional statistics are similar to those observed at higher Reynolds numbers in the atmosphere. A key requirement of the analysis to follow is that there must be a sufficiently broad scaling range in the temperature spectrum so that the statistics are independent of both the small scale (smearing or dissipation of the scalar) and the large scale forcing. Figure 2 shows the temperature spectrum at the position ($x/M = 62$) where the two and three-point statistics were obtained. The Reynolds number, R_λ, is 247. The Péclet number, $\mathrm{Pe}_\lambda \equiv (\nu/\kappa)R_\lambda$ (where κ is the thermal diffusivity) is 173. Also shown is the longitudinal velocity spectrum at the same position. Note that the temperature and velocity spectra have well developed scaling regions. The slope of the velocity spectrum in the inertial subrange is -1.52 and that of the temperature spectrum is -1.55, i.e., both are close to the Kolmogorov value of -1.67. (The R_λ and Pe_λ dependence of the spectral slope is discussed in M&W.[20]) The bulk of the analysis will be done for $R_\lambda = 213$, but in Sec. IV we will

TABLE I. Shown are the flow parameters for the primary cases for which results are presented in this paper. The two-point statistics were determined from the horizontal tunnel data for which the range of transverse separations extended to an integral scale. The three point statistics were mostly determined from the vertical tunnel data. The kinematic viscosity, ν, was 15×10^{-6} m^2/s. The thermal diffusivity, κ, was 22.5×10^{-6} m^2/s.

Speed (m/s)	6.0	12.5	13.3
Mode	Synchronous	Synchronous	Random
Tunnel	Horizontal	Vertical	Vertical
x/M	62	68	68
β (K/m)	3.7	3.9	2.6
$\langle u^2\rangle$ (m^2/s^2)	0.100	0.329	1.38
$\langle u^2\rangle^{1/2}/U$ (%)	5.3	2.6	10.4
$\epsilon (=15\nu\int_0^\infty k_1^2 F_{11}(k_1)dk_1)$ (m^2/s^3)	0.164	2.39	8.64
$l (=0.9\langle u^2\rangle^{3/2}/\epsilon)$ (m)	0.17	0.071	0.17
$R_\lambda (=\langle u^2\rangle\{15/(\nu\epsilon)\}^{1/2})$	247	213	469
$R_l (=\langle u^2\rangle^{1/2} l/\nu)$	3600	2700	13300
$\eta (=(\nu^3/\epsilon)^{1/4})$ (mm)	0.38	0.19	0.14
ϵ_θ [see Eq. (8) of M&W] (K^2/s)	0.581	0.173	0.136
$\langle\theta^2\rangle$ (K^2)	0.336	0.0405	0.0414
$l_\theta (=\langle\theta^2\rangle^{1/2}/\beta)$ (m)	0.16	0.052	0.078
Transverse probe separations (y/l)	0.012–0.75	0.014–0.13	0.043

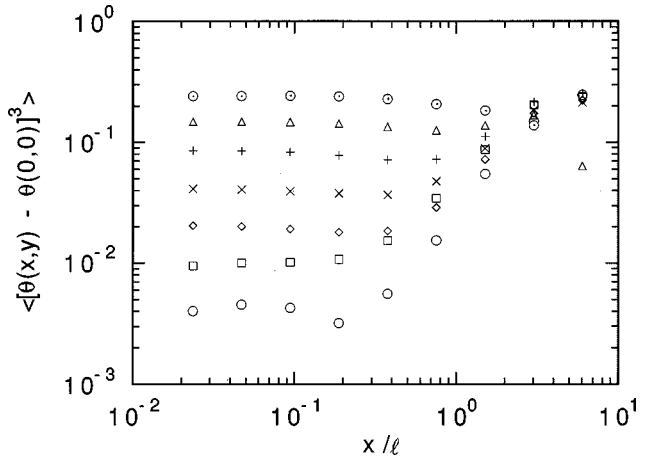

FIG. 3. The third order diagonal structure function of temperature at $R_\lambda = 247$ (horizontal tunnel, synchronous mode), $\langle(\Delta_{x,y}\theta)^3\rangle$, plotted as a function of x/l, where $x=Ut$ and l is the integral length scale. Different symbols correspond to different transverse separations: $\bigcirc, y/l=0.012$; $\square, y/l=0.024$; $\diamond, y/l=0.047$; $\times, y/l=0.094$; $+, y/l=0.19$; $\Delta, y/l=0.38$; $\odot, y/l=0.75$.

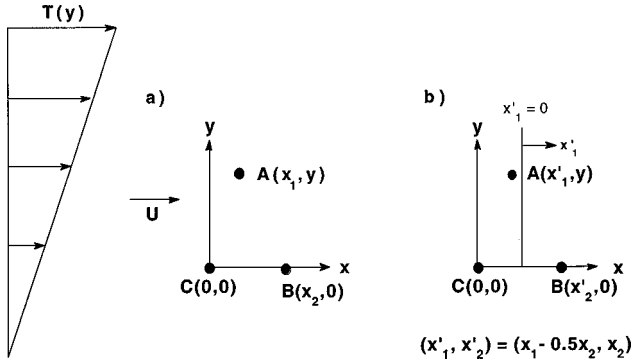

FIG. 4. Schematic and definitions of the labels and coordinates used in the discussion of three-point scalar statistics. U is the mean velocity of the air in the wind tunnel. θ are the fluctuations in temperature (Θ) about their mean, $T=T(y)$. There are two temperature probes placed at (0,0) and $(0,y)$. The coordinate system in (b) is introduced in Sec. III B.

show that similar results are obtained when the Reynolds number is doubled ($R_\lambda = 469$). Further, we will vary the spacing of the probes and show that the results are independent of the inertial-convective spacing. The flow parameters are listed in Table I.

Before we discuss the results of the three-point statistics of the temperature field, we will summarize the salient properties of the two-point statistics.

A. Two-point statistics

In Fig. 1, we showed that the transverse skewness structure function violates Kolmogorov scaling. Its lack of y-dependence implies that the derivative skewness is constant with Reynolds number and this has been verified by M&W for the constant mean temperature gradient case addressed here.

To help bridge the gap between two-point, one-dimensional statistics (such as the transverse structure function) and three-point (and therefore two-dimensional) statistics, we first present two-point, two-dimensional statistics, or what we call the diagonal (third-order) structure function, defined as

$$\langle(\Delta_{x,y}\theta)^3\rangle \equiv \langle[\theta(x=Ut,y)-\theta(0,0)]^3\rangle = \langle[\theta_A-\theta_C]^3\rangle. \tag{6}$$

It is plotted in Fig. 3 for various separations, y, as a function of x/l, where l is the integral length scale defined as $l = 0.9\langle u^2\rangle^{3/2}/\epsilon$ [Eq. (12) of Mydlarski and Warhaft.[4]] A sketch of the coordinate system is shown in Fig. 4(a) ($x = x_1$ here). (Point B and its corresponding coordinate, x_2, will be used later when discussing three-point statistics.) Data are shown for values of y/l ranging from 0.012 to 0.75 for $R_\lambda = 247$. In the limit of zero separation in the x-direction, this plot simply shows the transverse third-order structure function of temperature. Since the data of Fig. 3 are constant up to a value of $x/l \sim 1$, the width (x-extent) of a ''ramp-cliff'' structure is on the order of an integral scale. Thus, the ''ramp-cliff'' structures are large-scale features, yet as we have shown above, they are also manifested at the small scales. It appears that for the smallest separations (Fig. 3), the ramp-cliff structures are less wide than for the largest separations since the value of $\langle(\Delta_{x,y}\theta)^3\rangle$ is constant up to a smaller value of x/l. In fact, this might be expected since, at large x/y the diagonal structure function becomes experimentally indistinguishable from the longitudinal structure function and the transverse component of the signal may be prematurely ''lost.''

Although the temperature profile is roughly linear and (almost) constant,[20] the turbulence is decaying in the downstream (x) direction. In ideal, homogeneous flow, the third-order statistics should be even in x.[35] As a test of the effects of inhomogeneity, the third-order diagonal structure function is plotted as a function of x and $-x$ (Fig. 5) for a subset of the data of Fig. 3. For scales less than the integral length scale, the collapse is good implying that the statistics are even in the x-direction. In the work to follow, we only con-

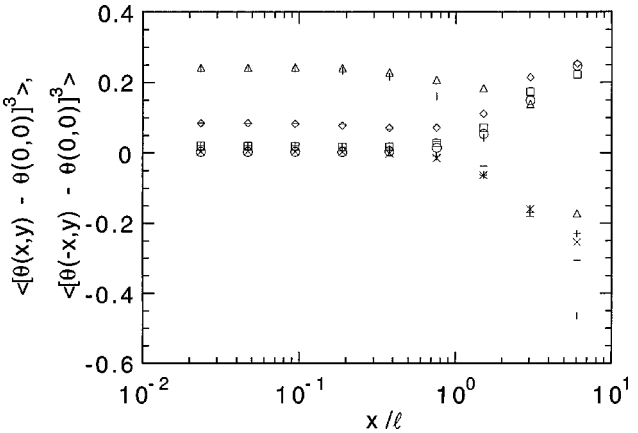

FIG. 5. The effect of a coordinate reflection in x on the third order diagonal structure function of temperature. $\langle(\Delta_{x,y}\theta)^3\rangle$ and $\langle(\Delta_{-x,y}\theta)^3\rangle$ are plotted as a function of x/l for various spacings at $R_\lambda = 247$ (horizontal tunnel, synchronous mode). Different symbols correspond to different transverse separations. In the positive x-direction, $\bigcirc, y/l=0.012$; $\square, y/l=0.047$; $\diamond, y/l=0.19$; $\triangle, y/l=0.75$. In the negative x-direction, $\times, y/l=0.012$; $+, y/l=0.047$; $-, y/l=0.19$; $|, y/l=0.75$.

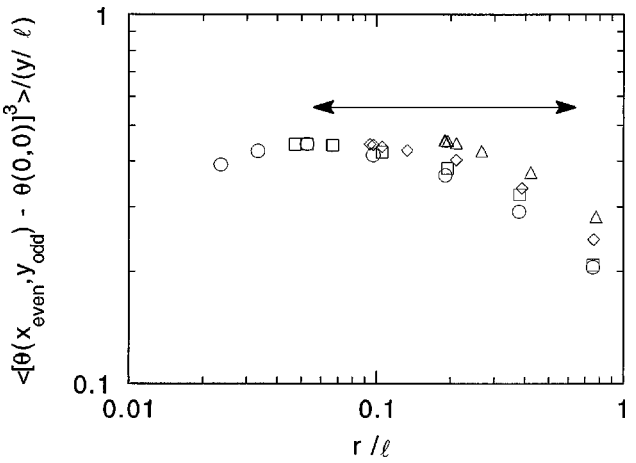

FIG. 6. The component of the diagonal third order structure function of temperature which is even in x and odd in y, $\langle(\Delta_{x_{\text{even}},y_{\text{odd}}}\theta)^3\rangle$, plotted as a function of r/l, where $r=(x^2+y^2)^{1/2}$ and scaled by y/l for inertial range separations of y. $R_\lambda=247$ (horizontal tunnel, synchronous mode) and different symbols correspond to different transverse separations; ○, $y/l=0.024$; □, $y/l=0.047$; ◇, $y/l=0.094$ and △, $y/l=0.19$. The horizontal arrow indicates the extent of the inertial-convective subrange determined from the second order longitudinal structure function.

sider the components of the statistics which are even in x to improve scaling. This precludes contamination from the largest, inhomogeneous scales which are odd in x. The even in x component of a statistic was calculated as follows (where we use the diagonal third-order structure function as an example): $\langle(\Delta_{x_{\text{even}},y}\theta)^3\rangle\equiv\frac{1}{2}(\langle(\Delta_{x,y}\theta)^3\rangle+\langle(\Delta_{-x,y}\theta)^3\rangle)$. Similarly, the third-order statistics should be odd in y.[35] [If you flip the direction of the gradient (hotter air below) the sign of the third-order statistics must change.] A similar test of the odd symmetry in y was performed. It verified that the data was indeed odd in y for separations up to an integral scale. Still, we will only consider the component of the statistics which is odd in y (and even in x) to prevent contamination from large scale inhomogeneities (such as small curvatures in our ideally linear gradient). Calculation of the component which was odd in y was done in an analogous manner to the calculation of the component which was even in x.

In Fig. 6, we show the component of the third-order diagonal structure function of temperature which is even in x and odd in y. It is shown to be approximately independent of $r(\equiv[x^2+y^2]^{1/2})$ when scaled by y. This graph is the same as in Fig. 18(a) of M&W.[20] We will return to it below.

B. The three-point statistics

We begin our discussion of three-point statistics by defining the variables used to describe the orientation of the three points. We consider three points, to be called A, B, and C, and we give them the coordinates $A=(x_1,y)$, $B=(x_2,0)$, and $C=(0,0)$ (see Fig. 4). In fact, only two cold-wires are used to measure temperature. T_B and T_C are determined from the same temperature signal in conjunction with Taylor's hypothesis to convert temporal increments into spatial ones. We note that Taylor's hypothesis should hold well in this low turbulence intensity ($\langle u^2\rangle^{1/2}/U<0.1$) isotropic velocity field.

Our objective is to arrive at the three-point correlation function or the equivalent ''three-point structure function.'' (These are two equivalent ways of expressing the same information.) We will consider what we call ''three-point structure functions'' rather than three-point correlations since we found that drift and inhomogeneity in the direction of the temperature gradient introduced error in the three-point measurements that was of the same order as the magnitude of the three-point correlation. (Forcing even symmetry in x and odd symmetry in y does not eliminate all inhomogeneities; the field may have inhomogeneities with these symmetries.) However, the size of the error amounted to a much smaller fraction of the signal in the three-point structure function. This might be expected since there exists inherent filtering in the calculation of a structure function (due to the fact that a subtraction is performed). The effect of drift on correlations is discussed in Lumley and Panofsky,[36] p. 44. They show that the effect of a (linear) trend (in time) in the data results in the autocorrelation having an error which is a function of the averaging time (T) squared. When considering (second-order) structure functions, the error term resulting from the trend is now only a function of the time lag (τ) squared (which is much more acceptable since $\tau/T\ll 1$).

We begin by considering one of many possible three-point structure functions,

$$S_1\equiv\langle(\theta_A-\theta_C)^2(\theta_A-\theta_B)\rangle. \tag{7}$$

It is emphasized that local isotropy predicts that S_1 should be zero at small scales for high Reynolds numbers. Given S_1, one can deduce the three-point correlation, $\langle\theta_A\theta_B\theta_C\rangle$. Consider the algebraic expansion of this three-point structure function into a sum of one-point, two-point, and (the desired) three-point third-order correlations,

$$\begin{aligned}\langle(\theta_A-\theta_C)^2(\theta_A-\theta_B)\rangle=&\langle\theta_A^3\rangle-2\langle\theta_A^2\theta_C\rangle+\langle\theta_A\theta_C^2\rangle\\&-\langle\theta_A^2\theta_B\rangle-\langle\theta_C^2\theta_B\rangle\\&+2\langle\theta_A\theta_B\theta_C\rangle.\end{aligned} \tag{8}$$

The correlations can also be divided in two types; those involving a separation in y and those which do not. The latter (ones which involve only one point, e.g., $\langle\theta_A^3\rangle$, and ones which only involve θ_B and θ_C, e.g., $\langle\theta_C^2\theta_B\rangle$), having no transverse component, should ideally be zero. Those involving θ_A and θ_B or θ_A and θ_C, can simply be re-expressed in terms of the third-order, two-point diagonal structure function, since it can be expanded as follows:

$$\langle(\theta_A-\theta_C)^3\rangle=\langle\theta_A^3\rangle-\langle\theta_C^3\rangle+3(\langle\theta_A\theta_C^2\rangle-\langle\theta_A^2\theta_C\rangle). \tag{9}$$

Assuming homogeneity of the temperature statistics and assuming even symmetry in x and odd symmetry in y, one obtains

$$\langle(\theta_A-\theta_C)^3\rangle|_{x_1,y}=6\langle\theta_A\theta_C^2\rangle=-6\langle\theta_A^2\theta_C\rangle, \tag{10}$$

$$\begin{aligned}\langle(\theta_A-\theta_B)^3\rangle&=\langle(\theta_A-\theta_C)^3\rangle|_{x_1-x_2,y}\\&=6\langle\theta_A\theta_B^2\rangle=-6\langle\theta_A^2\theta_B\rangle.\end{aligned} \tag{11}$$

One can therefore estimate the three-point correlation, $\langle \theta_A \theta_B \theta_C \rangle$, from S_1 and a curve fit to the diagonal structure function (Fig. 6) for the two-point, third order correlations [Eqs. (10) and (11)]. Thus,

$$\langle \theta_A \theta_B \theta_C \rangle|_{x_1,x_2,y} = \tfrac{1}{2}[\langle (\theta_A-\theta_C)^2(\theta_A-\theta_B)\rangle|_{x_1,x_2,y} - \tfrac{1}{2}\langle (\theta_A-\theta_C)^3\rangle|_{x_1,y} - \tfrac{1}{6}\langle (\theta_A-\theta_C)^3\rangle|_{x_1-x_2,y}]. \quad (12)$$

There also exists many alternate structure function definitions, e.g., $S_2 \equiv \langle (\theta_A-\theta_C)^2(\theta_C-\theta_B)\rangle$ from which $\langle \theta_A \theta_B \theta_C \rangle$ can be deduced. S_1 has been computed and will be discussed in the appendix. There, we will show that $\langle \theta_A \theta_B \theta_C \rangle$ derived from S_1 lacks the correct symmetry properties and shows unacceptable probe spacing dependence.

Here, following a suggestion of Shraiman, we choose the somewhat unusual combination

$$S \equiv \tfrac{1}{16}\langle 3(\theta_B+\theta_C-2\theta_A)(\theta_B-\theta_C)^2 - \tfrac{1}{3}(\theta_B+\theta_C-2\theta_A)^3\rangle. \quad (13)$$

To explain this choice, we expand S as follows:

$$S = \langle \theta_A \theta_B \theta_C \rangle + \tfrac{1}{3}\langle \theta_A^3+\theta_B^3+\theta_C^3\rangle - \tfrac{1}{12}\langle (\theta_A+\theta_B)^3 + (\theta_A+\theta_C)^3+(\theta_C+\theta_B)^3\rangle. \quad (14)$$

Note that S is permutationally symmetric, i.e., exchanging any two points (e.g., θ_A with θ_B, θ_A with θ_C, etc.) does not change the function. The triple correlation, $\langle \theta_A \theta_B \theta_C \rangle$, is also obviously permutationally symmetric. Therefore, in addition to the imposed even symmetry in x and the odd symmetry in y, we are now also (implicitly) imposing permutational symmetry by use of combination S. These three symmetries are all consistent with the required theoretical behavior of $\langle \theta_A \theta_B \theta_C \rangle$. [We remark that combination S_1 is not permutationally symmetric, see Eq. (8). Though the left-hand side of Eq. (12) is, the individual terms we measure on the right-hand side are not.]

Simplifying (14) by use of (10) and (11), we obtain

$$S = \langle \theta_A \theta_B \theta_C \rangle + \tfrac{1}{6}\langle \theta_A^3+\theta_B^3+\theta_C^3\rangle. \quad (15)$$

We observe that the structure function S is equivalent to the third-order three-point correlation, $\langle \theta_A \theta_B \theta_C \rangle$, to within the scalar (signal) skewness (which should be zero). Therefore, we measure a permutationally symmetric structure function to obtain the (permutationally symmetric) triple correlation.

Note that combination S does not require two-point statistics (such as $\langle \theta_A \theta_C^2 \rangle$ or $\langle \theta_A \theta_B^2 \rangle$) to be added or subtracted to obtain $\langle \theta_A \theta_B \theta_C \rangle$ as was the case with S_1 in Eq. (12). In addition, the assumption that $\langle \theta_B \theta_C^2 \rangle = \langle \theta_B^2 \theta_C \rangle = 0$ is no longer required. This was found to introduce error for larger separations in the calculation of $\langle \theta_A \theta_B \theta_C \rangle$ from other combinations.

As for many physical phenomena, the laboratory coordinates, namely (x_1, x_2, y), are not the optimal choice for representation of the three-point structure functions. When plotted as a function of x_1/y and x_2/y, the contour plots exhibited symmetries about the line $x_2 = 2x_1$. This is physically reasonable since when $x_2 = 2x_1$, the x-coordinate of point A is located midway between those of points B and C. In other words, the points A, B, and C form an isosceles triangle. We therefore choose (consistent with Mydlarski *et al.*[37]) to plot our contour plots in a modified coordinate system, $(x_1', x_2') = (x_1 - \frac{1}{2}x_2, x_2)$, see Fig. 4(b). This new choice of coordinates results in the $x_2 = 2x_1$ line of symmetry being transformed to the vertical, (x_2'), axis (i.e., the line $x_1' = 0$).

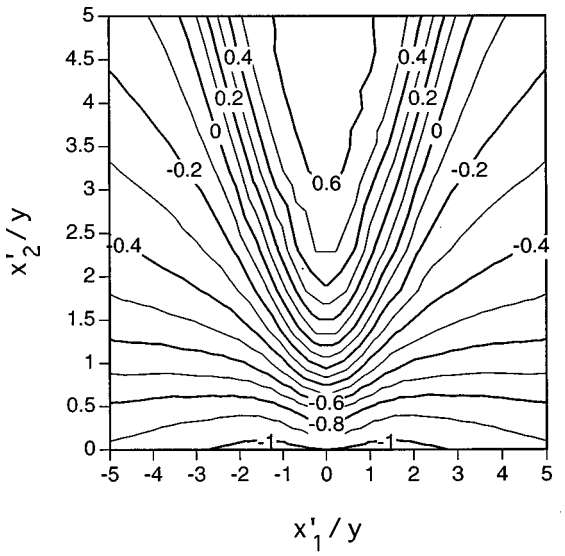

FIG. 7. Contour plot of the three-point triple correlation, $\langle \theta_A \theta_B \theta_C \rangle$, in (x_1', x_2') space as deduced from the three-point (third-order) scalar structure function for combination S. The transverse separation is 3.6 mm (i.e., $y/l = 0.051$) and $R_\lambda = 213$ (vertical tunnel, synchronous mode). The data are normalized by $-\langle \theta_A \theta_B \theta_C \rangle(0,0)$ at the given transverse separation.

Figure 7 shows the three-point third-order correlation, $\langle \theta_A \theta_B \theta_C \rangle$, calculated from combination S for a transverse spacing of $y = 3.6$ mm. It is plotted as a function of x_1'/y and x_2'/y. This plot is shown for the ranges $-5 < x_1'/y < 5$ and $0 < x_2'/y < 5$. (Since the statistics are even in x, it is unnecessary to show the range $-5 < x_2'/y < 0$, which will be identical to what is shown. Additionally, $\langle \theta_A \theta_B \theta_C \rangle$ is even in x_1',[35] therefore we only need to show data in the range $0 < x_1'/y < 5$ and $0 < x_2'/y < 5$. However, we show both halves of the plot to emphasize this latter symmetry.) The nondimensionalization is by $-\langle \theta_A \theta_B \theta_C \rangle|_{x_1'=0, x_2'=0} = -\langle \theta_A \theta_C^2 \rangle|_{x_1'=0}$. Therefore, the triple correlation must be equal to -1 for $(x_1', x_2') = (0,0)$. In addition, $\langle \theta_A \theta_B \theta_C \rangle$ must be zero when the three points form an equilateral triangle.[37] Therefore, the triple correlation must be equal to zero when $(x_1'/y, x_2'/y) = (0, 2/\sqrt{3}) \approx (0, 1.15)$. (When $x_1' = 0$, the triangle is isosceles. If $x_2' = 2/\sqrt{3}$ the triangle is then also equilateral.) We observe this to be the case. For values of $x_1' = 0$ and $x_2' > 2/\sqrt{3}$ the triple correlation becomes positive. Further elucidation of the nature of these three-point statistics and their relationship to the ramp-cliff structures is more easily done in terms of the structure function, and thus is addressed in the Appendix.

IV. PROBE SEPARATION AND REYNOLDS NUMBER DEPENDENCE

The principal result of this paper is the third-order correlation function shown in Fig. 7. It is the most general sta-

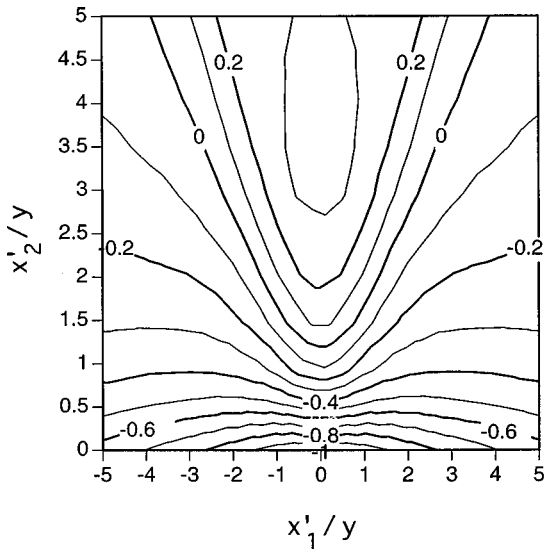

FIG. 8. The effect of a larger transverse separation on the contour plot of the three-point triple correlation, $\langle \theta_A \theta_B \theta_C \rangle$, in (x_1', x_2') space as deduced from combination *S*. The transverse separation is 9 mm (i.e., $y/l = 0.13$) and $R_\lambda = 213$ (vertical tunnel, synchronous mode). The data are normalized by $-\langle \theta_A \theta_B \theta_C \rangle(0,0)$ at the given transverse separation.

tistical description (at the third order) of the ramp-cliff structures that appear to be ubiquitous to all scalars mixed against a mean gradient by turbulence. In this section, we consider the effects of probe spacing (y) and Reynolds number.

In Fig. 8, we show $\langle \theta_A \theta_B \theta_C \rangle$, calculated from combination *S* for a transverse spacing of $y = 9$ mm. (Figure 7 was calculated for $y = 3.6$ mm.) There do exist some differences, such as the ''opening up'' of the V-shape (consider, for example, the -0.2 contour line) or the reduction in the maximum value achieved (from ~ 0.6 for $y = 3.6$ mm to ~ 0.3 for $y = 9$ mm). The overall result (including the constraint of $\langle \theta_A \theta_B \theta_C \rangle = 0$ when $(x_1'/y, x_2'/y) = (0, 2/\sqrt{3})$) is very consistent. Some differences should be expected at the larger spacing considering that an intermediate distance in Fig. 8 (of say, $3y = 3 \times 9$ mm $= 27$ mm) is close to an integral scale, which for this flow was 71 mm (and therefore $3y \sim 0.4l$).

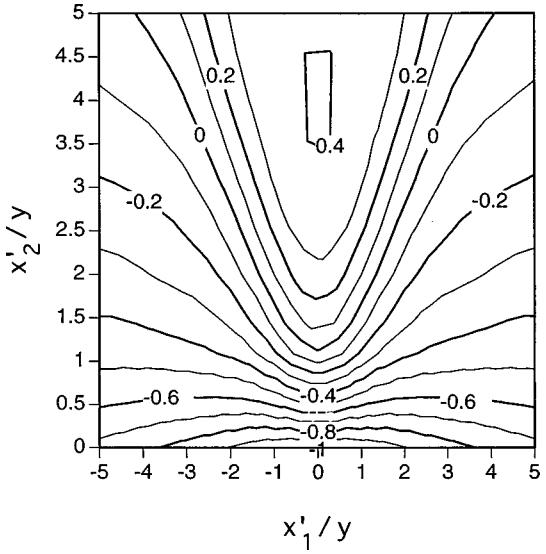

FIG. 9. The effect of Reynolds number on the contour plot of the three-point triple correlation, $\langle \theta_A \theta_B \theta_C \rangle$, in (x_1', x_2') space as deduced from combination *S*. The transverse separation is 7.35 mm (i.e., $y/l = 0.043$) and $R_\lambda = 469$ (vertical tunnel, random mode). The data are normalized by $-\langle \theta_A \theta_B \theta_C \rangle \times (0,0)$ at the given transverse separation.

Finally, we examine the effects of varying the Reynolds number. The triple correlation, $\langle \theta_A \theta_B \theta_C \rangle$ determined from combination *S*, is shown in Fig. 9 at $R_\lambda = 469$ obtained by operation of the active grid in the random mode.[4] (The majority of our runs in this paper have been performed with the grid in the synchronous mode for the reasons given in Sec. II. In that mode, the Reynolds number was 213.) Here the transverse separation was 7.35 mm. (The integral scale for this case, l, was 170 mm and the Kolmogorov microscale, η was 0.14 mm.) The results are very consistent with those of Fig. 7 indicating their lack of sensitivity to the Reynolds number. We note [M&W (Ref. 20)] that in the random mode there is a significant weakening of the mean temperature gradient with downstream distance, x. As a result, this diminished the value of the transverse derivative skewness,[20] $S_{\partial\theta/\partial y}$. However, the triple correlation appears to be unaffected, thus providing strong confirmation for the robustness of these results.

V. CONCLUSIONS

We have computed the third-order three-point correlation, $\langle \theta_A \theta_B \theta_C \rangle$, for a linear temperature profile in decaying grid turbulence. We show that is has a characteristic V-shape that is independent of Reynolds number over the range $213 \leqslant R_\lambda \leqslant 469$ $(2700 \leqslant R_l \leqslant 13300)$ and for probe separations less than an integral scale. Because the scalar skewness persists to very high Reynolds numbers,[18,20] it may be reasonably inferred that so too will be the V-shaped three-point correlation, since it represents the ramp-cliff structures that are responsible for the skewness. We note that since the ramp-cliff structures have been observed in both shear[16–18] and shear-free[21] flows, and that the third-order two-point structure function scales similarly for both types of flows,[17,20] this suggests that our results may indeed be universal to all turbulent flows with a mean temperature gradient.

In another paper,[37] our measurements will be compared with the predictions of Shraiman, Siggia, and Pumir[24–27] who determine the same three-point functions using the Hopf equation as the basis for their model. In the present work, it has been our objective to describe the way in which we have arrived at the three-point statistics, and what variation they exhibit with various parameters, rather than to compare with predictions.

ACKNOWLEDGMENTS

We thank Professor E. D. Siggia, Professor A. Pumir, and Dr. B. I. Shraiman for providing the motivation for this work and for many discussions. As always, we thank E. P. Jordan for his most helpful technical assistance. The work was supported by the Department of Energy (Basic Energy Sciences).

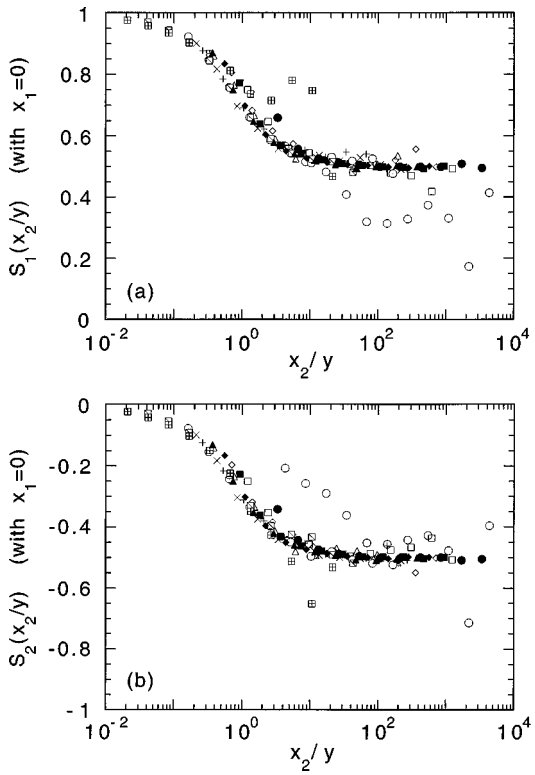

FIG. 10. The right-angle three-point (third-order) scalar structure functions (i.e., three-point scalar structure functions with $x_1=0$) plotted against x_2/y for combinations S_1 (a) and S_2 (b). Solid symbols are for $R_\lambda=213$ (vertical tunnel, synchronous mode) which correspond to different transverse separations; solid circles are $y/l=0.014$; solid squares are $y/l=0.051$; solid diamonds are $y/l=0.085$, and solid triangles are $y/l=0.13$. Remaining symbols are for $R_\lambda=564$ (horizontal tunnel, random mode); open circles are $y/l=0.0026$; open squares are $y/l=0.0092$; open diamonds are $y/l=0.016$; open triangles are $y/l=0.029$; plus signs are $y/l=0.042$; crosses are $y/l=0.052$; circles with dots are $y/l=0.068$; squares with slashes are $y/l=0.27$ and squares with plus signs are $y/l=0.53$. The data are normalized by the value of the transverse third-order structure function for their respective transverse separation.

APPENDIX: THREE-POINT STRUCTURE FUNCTIONS

Given the triple correlation, $\langle\theta_A\theta_B\theta_C\rangle$, one can extract any possible third-order structure function. Rather than estimating these from the triple correlation, in this appendix we will present some (directly measured) three-point structure functions. We examine (two possible combinations of) third-order three-point structure functions. These combinations, labeled S_1 and S_2, were mentioned in Sec. III B and are redefined below,

$$S_1\equiv\langle(\theta_A-\theta_C)^2(\theta_A-\theta_B)\rangle, \tag{A1}$$

$$S_2\equiv\langle(\theta_A-\theta_C)^2(\theta_C-\theta_B)\rangle. \tag{A2}$$

We emphasize, as a generalization of (3), that S_1 and S_2 should be zero at small scales for high Reynolds numbers. Many other possible combinations exist, but they can all be expressed in terms of S_1 and/or S_2.

The first type of three-point structure function we consider is the ''right-angle three-point structure function'' in which the three points form a right angle by enforcing that $x_1=0$ [i.e., only x_2 and y will be allowed to vary, Fig. 4(a)]. Figures 10(a) and 10(b) show the right-angle three-point structure function for combinations S_1 and S_2 for a wide variety of transverse separations y. (A discussion of the right-angle three-point structure function is more reasonably done in the laboratory coordinate system. We therefore return to it temporarily.) The curves in Fig. 10 collapse very well. The few data points which do not follow the general trend are found to be for the smallest and largest transverse spacings, which are well out of the inertial range. Here we have included data from the vertical tunnel as well as some data recorded in our horizontal tunnel (for which the data records were not as long as for those measured in the vertical tunnel). In addition, these figures show no dependence on the mode of operation of our active grid (viz., synchronous or random) and therefore no dependence on Reynolds number.

In these figures, the ordinate is normalized by the value of the transverse third-order (two-point) structure function for the given transverse spacing, y. Consequently, the right-angle three-point structure functions for combination S_1 must tend to 1 in the limit of $x_2\to 0$ since, in this limit, $\theta_B\to\theta_C$, and therefore combination S_1 becomes $\langle(\theta_{A|_{x_1=0}}-\theta_C)^3\rangle$, which is the definition of the transverse third-order structure function. The fact that $\theta_B\to\theta_C$ as $x_2\to 0$ also explains why the right-angle three-point structure function for combination S_2 tends to zero in the limit $x_2\to 0$. The abscissa is normalized by y so that the triangles (defined by the three positions at which the temperature is measured in these structure functions) are all similar (in the geometrical sense).

At large separations, the data asymptotes to 0.5 in Fig. 10(a) and -0.5 in Fig. 10(b). These can be predicted from an (algebraic) expansion of S_1 and S_2 which shows that there are some terms which do not go to zero as $x_2/y\to\infty$ (i.e., the third-order correlations which do not contain θ_B, e.g., $\langle\theta_{A|_{x_1=0}}\theta_C^2\rangle$). Recall that we are nondimensionalizing by $\langle(\theta_{A|_{x_1=0}}-\theta_C)^3\rangle$ which is equal to $6\langle\theta_{A|_{x_1=0}}\theta_C^2\rangle$ $(=-6\langle\theta_{A|_{x_1=0}}^2\theta_C\rangle)$. The asymptote quantifies the contribution to the structure function from correlations independent of θ_B.

The next step is to remove the $x_1=0$ restriction. Instead, we let x_1 be a third independent variable (along with x_2 and y). The resulting three-point structure functions (for a given combination) must then be plotted as contour plots as a function of x_1/y and x_2/y for a given transverse spacing, y. Here we also return to the coordinate system denoted by primes.

Figures 11(a) and 11(b) show the three-point structure functions for combinations S_1 and S_2 for a transverse spacing of $y=3.6$ mm. These plots are shown for the ranges $-5<x_1'/y<5$ and $0<x_2'/y<5$. (Since the statistics are even in x, it is unnecessary to show the range $-5<x_2'/y<0$, which will be identical to what is shown.) The nondimensionalizations are the same as for the right-angle three-point structure functions shown in Fig. 10. Combination S_1 must be equal to 1 at $(x_1'/y,x_2'/y)=(x_1/y,x_2/y)=(0,0)$. Since we only consider the component which is even in x, the statistics are even in x_1' when looking at the line $x_2'/y=0$. In addition, combination S_2 must also be zero along this line. We also remark that all the information (for a given transverse spacing) shown in Fig. 10 can be found in the, more general,

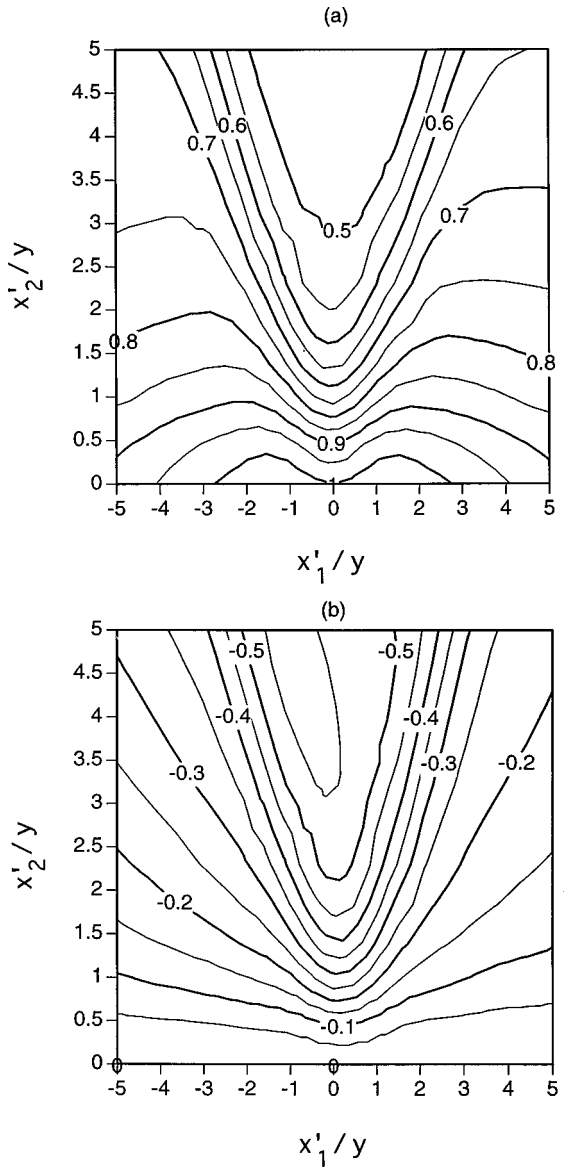

FIG. 11. Contour plots of the three-point (third-order) scalar structure functions in (x_1',x_2') space for combinations S_1 (a) and S_2 (b). The transverse separation is 3.6 mm (i.e., $y/l=0.051$) and $R_\lambda=213$ (vertical tunnel, synchronous mode). The data are normalized by the value of the transverse third-order structure function for the given transverse separation.

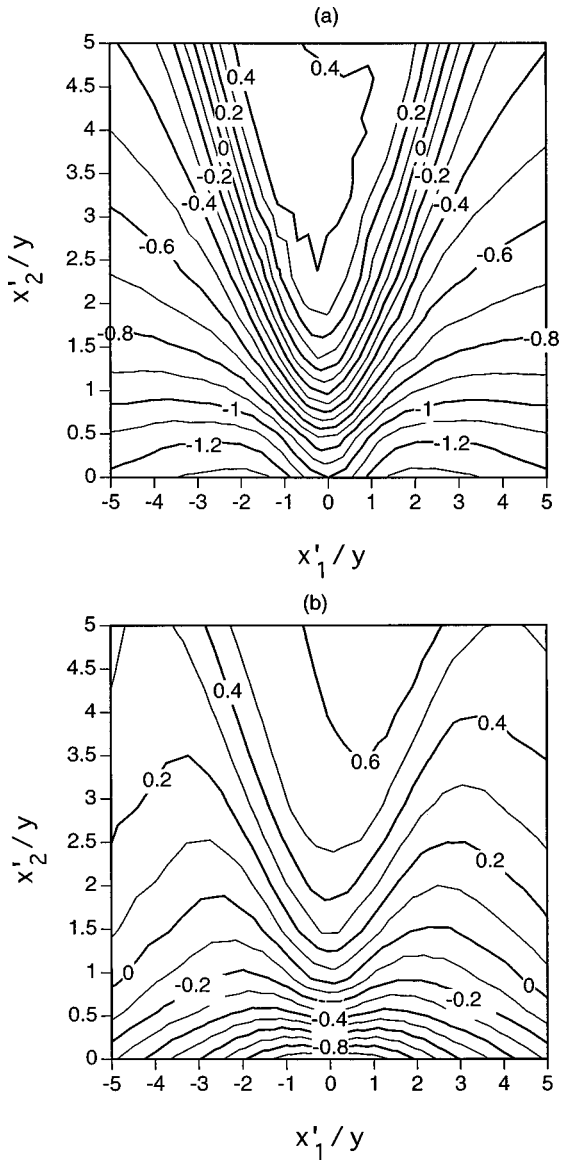

FIG. 12. The contour plot of the three-point triple correlation, $\langle \theta_A\theta_B\theta_C\rangle$, in (x_1',x_2') space as deduced from combination S_1. The transverse separation is (a) 3.6 mm (i.e., $y/l=0.051$) (b) 9 mm (i.e., $y/l=0.13$). $R_\lambda=213$ (vertical tunnel, synchronous mode). The data are normalized by $-\langle \theta_A\theta_B\theta_C\rangle(0,0)$ at the given transverse separation.

plots of Fig. 11 (for values of $x_2'/y<5$.) The right-angle three-point structure functions of Fig. 10 correspond to a cross section of the contour plots of Fig. 11 along the line given by $x_1'/y=-\frac{1}{2}x_2'/y$. (This corresponds to a vertical line given by $x_1/y=0$ in the laboratory coordinates.)

The magnitudes of the contour lines in Figs. 11(a) and 11(b) can be explained when one considers horizontal (x_2' = constant) cross sections of the plots. When $|x_1'|/|x_2'|\to\infty$, i.e. when point A is very far away from points B and C, points B and C become coincident. In this limit, S_1 reduces to the third-order diagonal structure function ($\langle(\theta_A-\theta_C)^3\rangle$) and should therefore be roughly 1. [For subintegral scale separations, the diagonal structure function shows little x-dependence (Fig. 6), and is therefore roughly equal to the value by which we are normalizing, the transverse structure function.] In this same limit, $S_2\to 0$ since B and C become indistinguishable. This is observed in Figs. 11(a) and 11(b). The limit $|x_1'|/|x_2'|\to\infty$ can be considered the one in which the triangle given by the three points is maximally skewed. In this limit, S_1 has a maximum (absolute) value and S_2 has a minimum (absolute) value. The opposite limit occurs when the x-coordinate of point A is located midway in between the x-coordinates of points B and C, and the triangle given by these three points is then isosceles (i.e., $x_1'=0$). This arrangement results in a minimum (absolute) value of S_1 and a maximum (absolute) value of S_2. The transition between these two limits, which results in V-shaped contour lines, is observed in Fig. 11. In Fig. 11(a), the contour lines for smaller x_2' overturn and depart from the predominant V-shape. We attribute this to large-scale effects. This does not

occur in Fig. 11(b) since the geometrical constraints imposed on combination S_2 (being zero along the $x_2'=0$ line) render this impossible.

We remark that combinations S_1 and S_2 are *not* even in x_1' (unlike the triple correlation $\langle \theta_A\theta_B\theta_C\rangle$) though they appear to be very close. In fact, the component of S_1 and S_2 which is odd in x_1' can be shown to be small,[35] but nonzero.

Finally, following the method of Eq. (12) and fitting a power law (of the form $\langle(\theta_A-\theta_C)^3\rangle|_{x_1,y}=Cy/(r^\alpha)$) to the inertial range of the third-order diagonal structure function (Fig. 6), we calculate the three-point triple correlation, $\langle \theta_A\theta_B\theta_C\rangle$, deduced from S_1. (The r^α term is a correction[37] to the assumed linear dependence of the third-order structure function on y. Since Fig. 6 is almost flat in the inertial range, α will be close to zero. Our experiments indicated values of α between 0.05 and 0.15. The small value of alpha is another way to show that the above mentioned asymmetry in x_1' of S_1 and S_2 is small. The component which is odd in x_1' disappears if $\alpha=0$ (Ref. 35)—this is not the case here.) In Figs. 12(a) and 12(b), we show $\langle \theta_A\theta_B\theta_C\rangle$, for a transverse spacing of $y=3.6$ mm and $y=9$ mm, respectively. Figure 12(a) is qualitatively similar to Fig. 7, though it can be observed that Fig. 7 (deduced from combination S) is in better accord with some of the theoretical requirements of $\langle \theta_A\theta_B\theta_C\rangle$ (i.e., it must be even in x_1', it must be zero for $(x_1'/y,x_2'/y)=(0,2/\sqrt{3})$, etc.). A quick examination of Fig. 12(b) will lead one to conclude that combination S_1 is much more sensitive to large-scale inhomogeneities than combination S. The similarity between Figs. 12(a) and 12(b) is much less than the similarity between Figs. 7 and 8. The more universal results obtained with combination S are attributed to the permutational symmetry implicit in its definition.

[1] A. N. Kolmogorov, ''The local structure of turbulence in incompressible viscous fluid for very large Reynolds numbers,'' Dokl. Akad. Nauk SSSR **30**, 301 (1941).

[2] A. N. Kolmogorov, ''Dissipation of energy in locally isotropic turbulence,'' Dokl. Akad. Nauk SSSR **32**, 16 (1941).

[3] S. G. Saddoughi and S. V. Veeravalli, ''Local isotropy in turbulent boundary layers at high Reynolds number,'' J. Fluid Mech. **268**, 333 (1994).

[4] L. Mydlarski and Z. Warhaft, ''On the onset of high Reynolds number grid generated wind tunnel turbulence,'' J. Fluid Mech. **320**, 331 (1996).

[5] A. N. Kolmogorov, ''A refinement of previous hypotheses concerning the local structure of turbulence in a viscous incompressible fluid at very high Reynolds numbers,'' J. Fluid Mech. **13**, 82 (1962).

[6] A. M. Oboukhov, ''Some specific features of atmospheric turbulence,'' J. Fluid Mech. **13**, 77 (1962).

[7] U. Frisch, *Turbulence: The Legacy of A.N. Kolmogorov* (Cambridge University Press, Cambridge, 1995).

[8] M. Nelkin, ''Universality and scaling in fully developed turbulence,'' Adv. Phys. **43**, 143 (1994).

[9] A. Pumir and B. I. Shraiman, ''Persistent small scale anisotropy in homogeneous shear flows,'' Phys. Rev. Lett. **75**, 3114 (1995).

[10] A. Pumir, ''Turbulence in homogeneous shear flows,'' Phys. Fluids **8**, 3112 (1996).

[11] S. Garg and Z. Warhaft, ''On the small scale structure of simple shear flow,'' Phys. Fluids **10**, 662 (1997).

[12] A. M. Oboukhov, ''Structure of the temperature field in turbulent flows,'' Izv. Akad. Nauk. SSSR, Geogr. Geofiz. **13**, 58 (1949).

[13] S. Corrsin, ''On the spectrum of isotropic temperature fluctuations in isotropic turbulence,'' J. Appl. Phys. **22**, 469 (1951).

[14] N. N. Korchashkin, ''The effect of fluctuations of energy dissipation and temperature dissipation on locally isotropic turbulent fields,'' Izv. Acad. Sci. USSR Atmos. Oceanic Phys. **6**, 947 (1970).

[15] C. W. Van Atta, ''Influence of fluctuations in local dissipation rates on turbulent scalar characteristics in the inertial subrange,'' Phys. Fluids **14**, 1803 (1971); **16**, 574 (1971).

[16] C. H. Gibson, C. A. Friehe, and S. O. McConnell, ''Structure of sheared turbulent fields,'' Phys. Fluids Suppl. **20**, s156 (1977).

[17] R. A. Antonia and C. W. Van Atta, ''Structure functions of temperature fluctuations in turbulent shear flows,'' J. Fluid Mech. **84**, 561 (1978).

[18] K. R. Sreenivasan, ''On local isotropy of passive scalars in turbulent shear flows,'' Proc. R. Soc. London, Ser. A **434**, 165 (1991).

[19] C. Tong and Z. Warhaft, ''On passive scalar derivative statistics in grid turbulence,'' Phys. Fluids **6**, 2165 (1994).

[20] L. Mydlarski and Z. Warhaft, ''Passive scalar statistics in high-Péclet-number grid turbulence,'' J. Fluid Mech. **358**, 135 (1998).

[21] M. Holzer and E. D. Siggia, ''Turbulent mixing of a passive scalar,'' Phys. Fluids **6**, 1820 (1994).

[22] A. Pumir, ''A numerical study of the mixing of a passive scalar in three dimensions in the presence of a mean gradient,'' Phys. Fluids **6**, 2118 (1994).

[23] J. L. Lumley, ''Similarity and the turbulent energy spectrum,'' Phys. Fluids **10**, 855 (1967).

[24] B. I. Shraiman and E. D. Siggia, ''Anomalous scaling of a passive scalar in turbulent flow,'' C. R. Acad. Sci. **321**, 279 (1995).

[25] B. I. Shraiman and E. D. Siggia, ''Symmetry and scaling of turbulent mixing,'' Phys. Rev. Lett. **77**, 2463 (1996).

[26] A. Pumir, ''Determination of the three-point correlation function of a passive scalar in the presence of a mean gradient,'' Europhys. Lett. **37**, 529 (1997).

[27] A. Pumir, ''Structure of the three-point correlation function of a passive scalar in the presence of a mean gradient,'' Phys. Rev. E **57**, 2914 (1998).

[28] A. Sirivat and Z. Warhaft, ''The effect of a passive cross-stream temperature gradient on the evolution of temperature variance and heat flux in grid turbulence,'' J. Fluid Mech. **128**, 323 (1983).

[29] K. Yoon and Z. Warhaft, ''The evolution of grid-generated turbulence under conditions of stable thermal stratification,'' J. Fluid Mech. **215**, 601 (1990).

[30] H. Makita, ''Realization of a large-scale turbulence field in a small wind tunnel,'' Fluid Dyn. Res. **8**, 53 (1991).

[31] J. C. Wyngaard, ''Measurements of small-scale turbulence structure with hot wires,'' J. Sci. Instrum. **1**, 1105 (1968).

[32] J. Haughdal and J. H. Lienhard, ''A low-cost high-performance cold-wire bridge,'' J. Phys. E **21**, 167 (1988).

[33] J. C. Wyngaard, ''Spatial resolution of a resistance wire temperature sensor,'' Phys. Fluids **14**, 2052 (1971).

[34] L. W. B. Browne and R. A. Antonia, ''The effect of wire length on temperature statistics in a turbulent wake,'' Exp. Fluids **5**, 426 (1987).

[35] L. Mydlarski, Ph.D. dissertation, Cornell University, 1998.

[36] J. L. Lumley and H. A. Panofsky, *The Structure of Atmospheric Turbulence* (Wiley, New York, 1964).

[37] L. Mydlarski, A. Pumir, B. I. Shraiman, E. D. Siggia, and Z. Warhaft, ''Structures and multipoint correlators for turbulent advection: Predictions and experiments,'' to appear in Phys. Rev. Lett.